

Pre-Heated Isentropic Gas in Groups of Galaxies

Mike L. Balogh, Arif Babul, and David R. Patton¹

¹ *Department of Physics & Astronomy, University of Victoria, Victoria, BC, V8X 4M6, Canada*
Email: balogh, babul, patton@uvastro.phys.uvic.ca

11 November 2021

ABSTRACT

We confirm that the standard assumption of isothermal, shock-heated gas in cluster potentials is unable to reproduce the observed X-ray luminosity–temperature relation of groups of galaxies. As an alternative, we construct a physically motivated model for the adiabatic collapse of pre-heated gas into an isothermal potential that improves upon the original work of Kaiser (1991). The luminosity and temperature of the gas is calculated, assuming an appropriate distribution of halo formation times and radiation due to both bremsstrahlung and recombination processes. This model successfully reproduces the slope and dispersion of the luminosity–temperature relation of galaxy groups. We also present calculations of the temperature and luminosity functions for galaxy groups under the prescription of this model. This model makes two strong predictions for haloes with total masses $M < 10^{13} M_{\odot}$, which are not yet testable with current data: (1) the gas mass fraction will increase in direct proportion to the halo mass; (2) the gas temperature will be larger than the virial temperature of the mass. The second effect is strong enough that group masses determined from gas temperatures will be overestimated by about an order of magnitude if it is assumed that the gas temperature is the virial temperature. The entropy required to match observations can be obtained by heating the gas at the turnaround time, for example, to about 3×10^6 K at $z=1$, which is too high to be generated by a normal rate of supernova explosions. The isentropic model breaks down on the scale of low mass clusters, but this is an acceptable limitation, as we expect accretion shocks to contribute significantly to the entropy of the gas in such objects.

Key words: galaxies: clusters: general – intergalactic medium

1 INTRODUCTION

The abundance of virialised clusters and groups of galaxies can provide a sensitive probe of the amplitude of density fluctuations on different scales and, hence, can be used to determine cosmological parameters. This requires, however, a theoretical framework for relating observable quantities such as the X-ray luminosity (L) and temperature (T) of the intra-cluster or intra-group medium (hereafter referred to as the ICM in both cases, for simplicity) to the total mass of the structure. The most commonly applied model assumes that the gas has been shock heated to the virial temperature of the isothermal mass. This results in a scaling relation $L \propto T^2$ (Kaiser 1991; Eke et al. 1996), which does not match the observed relation for clusters, (approximately $L \propto T^3$ (Edge, Stewart 1991; Markevitch 1998)) or that of groups, which may be even steeper (Ponman et al. 1996). It is also true that the $L \propto T^2$ scaling does not require isothermal gas; we develop such a model in Appendix A.

It was originally shown by Kaiser (1991) that, if the gas was pre-heated (for example by supernova explosions) before falling into the dark matter potential, the observed cluster L – T relation can be more accurately reproduced. Assuming adiabatic collapse under these conditions, Kaiser’s self-similar model predicts $L \propto T^{3.5}$. However, in this case, the radial extent of the gas depends strongly on the size of the potential; for low mass groups, the gas will extend well beyond the virial radius and, for high mass clusters, it will be concentrated in the centre. This may result in unreasonable gas mass fractions within the virial radius.

Other authors have attempted variations on the self-similar model. Bower (1994) explored arbitrary scaling relations of the form $L \propto (1+z)^s M^p$, where s and p are free parameters, in an attempt to reduce the predicted

evolution of the X-ray luminosity function. A special case of this treatment is the model of Evrard & Henry (1991), which yields the relation $L \propto T^{11/4}$. Both of these models are based on the assumption that the core gas possesses a minimum entropy, the value of which is determined by the entropy of the initially pre-heated gas. Outside this core, it is assumed that the gas is distributed isothermally. However, the physical reality of a gas core has not yet been demonstrated, and the assumption of a largely isothermal profile may not be supported by observations (Markevitch et al. 1998). Furthermore, as noted by Ponman et al. (1996), this relation, when extrapolated to lower mass scales, does not fit the X-ray data of galaxy groups.

Recently, Cavaliere, Menci & Tozzi (1997; 1998), have constructed a model in which the observed L–T relation on both cluster and group scales can be reproduced by varying the gas density at the virial radius, according to the accretion-shock strength, as determined by the temperature difference between the infalling and virialised gases. In the present work, we explore the case in which pre-heated gas is assumed to collapse adiabatically, with the effect of shocks neglected. This is somewhat similar to the model of Cavaliere et al. on group scales, where shocks are expected to be weak, although we put physical constraints on the total gas mass within virialised haloes and do not require an isothermal distribution.

The paper is organised as follows. In § 2, our cosmological and structure formation parameters are defined. The specific models for the gas distributions are presented in § 3: in particular the isothermal model in § 3.1 and the isentropic model in § 3.2.3. The luminosity–temperature–mass relations and the temperature/luminosity functions are presented in § 4. The models are discussed in terms of their evolutionary predictions, energy requirements and failures in § 5. The conclusions are summarised in § 6.

2 THEORETICAL FRAMEWORK

2.1 Cosmological Parameters

We will restrict our analysis in the present work to two simple cosmologies: a standard cold dark matter (CDM) model with $\Omega_o = 1$, $h = 0.5$, and an open model with $\Omega_o = 0.3$, $h = 0.75$. The values of h are chosen so that the age of the universe is equal to about 13 Gyr in both models. Unless otherwise specified, the baryon fraction of the universe, Ω_b , will be given by the big bang nucleosynthesis value $\Omega_b = 0.0125h^{-2}$ (Copi, Schramm, Turner 1995).

A simple function is fit to the $z = 0$ variance of mass fluctuations, $\sigma(M, 0)$, from the CDM power spectrum (Bardeen et al. 1986) for the two cosmological models:

$$\log(\sigma(M, 0)/\sigma_8) = - \begin{cases} 0.0128 + 0.298 \log \frac{M}{M_8} + 0.0211 (\log \frac{M}{M_8})^2 & ; \Omega_o = 1 , \\ 0.017 + 0.248 \log \frac{M}{M_8} + 0.0187 (\log \frac{M}{M_8})^2 & ; \Omega_o = 0.3 \end{cases} \quad (1)$$

where the normalisation of the power spectrum is determined by the constant $\sigma_8 = \sigma(M_8)$, and $M_8 = \frac{4\pi}{3} \rho_c(0) \Omega_o (8h^{-1} \text{Mpc})^3 = 5.962 \times 10^{14} h^{-1} \Omega_o M_\odot$ is the mass within an $8h^{-1}$ Mpc sphere, with $\rho_c(0)$ representing the critical density at $z = 0$. These fits correspond to a spectral index n ($P(k) \propto k^n$) ranging from $n = -2$ at the low mass end to $n = -1$ for the largest masses considered in this work.

The linearly extrapolated value of $\sigma(M, 0)$ at a redshift z is $\sigma(M, z) = \sigma(M, 0)g(z)/g(0)$, where the growth term $g(z)$ is given, to a close approximation in the case of $\Omega_o < 1$ (Viana, Liddle 1996), by

$$g(z) = (1+z)^{-1} \begin{cases} 1 & \Omega_o = 1, \\ \frac{5}{2} \Omega(z) (1 + \frac{\Omega(z)}{2} + \Omega(z)^{4/7})^{-1} & \Omega_o < 1, \Lambda = 0 \end{cases} \quad (2)$$

where $\Omega(z) = \Omega_o(1+z)/(1+\Omega_o z)$.

2.2 Halo Formation Times

For a halo of a given mass, the density profile of the ICM is related to the shape and the depth of the gravitational potential, with the latter depending on the epoch of halo formation; haloes of a given mass that form at an earlier epoch are denser, and more compact. This effect has often been neglected in the past, but has been treated recently by Kitayama & Suto (1996a, 1996b). Numerical simulations (Navarro, Frenk, White 1995) suggest that the depth of the potential well, as traced by the circular velocity V_c , remains relatively unchanged after 75 per cent of the cluster mass is in place, since the rest will be accreted in minor merger events that do not significantly disrupt the mass already in place. Thus motivated, we will define the redshift of halo formation as the redshift at which 75 per cent of the mass has been assembled; the X-ray temperature of the gas corresponding to a halo of mass M at the epoch of observation will then be determined by the circular velocity of that halo when its mass was equal to $0.75M$. We

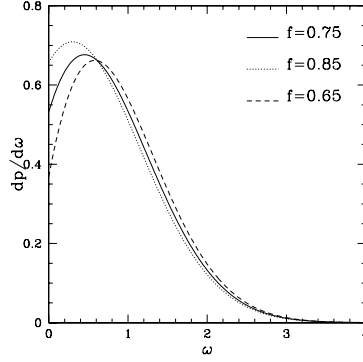


Figure 1. The probability distribution of halo formation times in the model of Lacey & Cole (1993), as parameterised by ω , which is related to the halo mass and redshift of formation as described in the text (§ 2.2). The three different curves correspond to three different definitions of halo formation; the factor f represents the fraction of the final mass (at the observed epoch) that is virialised at the epoch of formation.

will assume that both gas and dark matter components of merging haloes mix thoroughly and that the mixed gas immediately settles into hydrostatic equilibrium after a merger event.

An analytic description of halo formation times, applicable to any bottom-up hierarchical model in which structure formation is due to gravitational instability, was developed by Lacey & Cole (1993; 1994). For a halo of mass M , observed at redshift z , the probability that a fraction f of its mass was virialised at an earlier redshift z_f is

$$\frac{dp(z_f)}{dz_f} = \left[2\omega(f^{-1} - 1)\text{erfc}\left(\frac{\omega}{\sqrt{2}}\right) - \sqrt{\frac{2}{\pi}}e^{-\frac{\omega^2}{2}}(f^{-1} - 2) \right] \frac{d\omega}{dz_f}, \quad (3)$$

where the parameter ω is given by:

$$\omega(z_f) = \frac{g(0)}{g(z)} \frac{\delta_c(g(z)/g(z_f) - 1)}{\sqrt{\sigma^2(fM(z), 0) - \sigma^2(M(z), 0)}}. \quad (4)$$

Equation 3 is only strictly true for the special case $\sigma(M, 0) = \sigma_8 \left(\frac{M}{M_8}\right)^{-1/2}$, but the dependence on the shape of the power spectrum is weak (Lacey, Cole 1993) and so is neglected for simplicity. The dependence on the parameter f is shown in Figure 1; the most probable value of ω decreases from 0.6 to 0.3 as f increases from 0.65 to 0.85, but this has a negligible effect on the present calculations. The distribution of formation times, assuming $f=0.75$, is shown in Figure 2 for three representative mass scales at the present epoch, in both cosmological models. Lower mass haloes have a broader distribution of formation epochs, and haloes in the low density universe model form at earlier times, on average, than those in the critical density model. This analytic description of halo formation times has been shown to agree well with numerical simulations (Lacey, Cole 1994; Eke, Navarro, Frenk 1998).

2.3 Construction of the Temperature and Luminosity Functions

The comoving abundance of clusters as a function of mass can be determined using the Press–Schechter (1974) formalism (also Bond et al. 1991), which has been supported by some numerical simulations (Efstathiou, Bond, White 1992; White, Efstathiou, Frenk 1993; Lacey, Cole 1994; Eke et al. 1996) and is given by

$$\frac{dN(> M)}{dM} dM = \sqrt{\frac{2}{\pi}} \frac{\rho_c(0)\Omega_0\delta_c}{\sigma(M, z)^2 M} \exp\left(\frac{-\delta_c^2}{2\sigma(M, z)^2}\right) \left(-\frac{d\sigma(M, z)}{dM}\right) dM, \quad (5)$$

where $\delta_c = 1.686\Omega(z)^{0.0185}$ is the value of the linearly extrapolated critical overdensity for spherical gravitational collapse (corresponding to the top-hat filter) at redshift z , assuming no cosmological constant (Navarro, Frenk, White 1996). There is accumulating evidence (Bertschinger, Jain 1993; Governato et al. 1998; Somerville et al. 1998) that the shape of the mass function on the scales of groups and clusters, as determined from higher resolution numerical simulations, is not the same as that predicted by the Press–Schechter formalism. The differences amount to a factor of 2–3 on both high and low mass scales; nonetheless the Press–Schechter prediction will be used here, and a study of the error introduced by this procedure will be deferred.

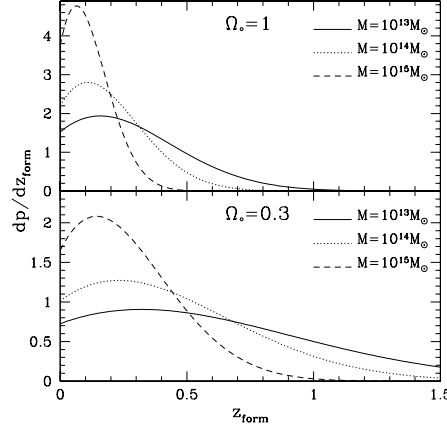


Figure 2. The probability distribution of halo formation times as a function of redshift in the model of Lacey & Cole (1993), for haloes at $z = 0$ with three different masses, assuming $f=0.75$. The top panel shows the results for $\Omega_o = 1$, while the bottom panel shows the results for $\Omega_o = 0.3$. Compared to high mass haloes, the low mass haloes have a higher most probable redshift of formation, as well as a broader distribution of formation times.

The differential temperature function is obtained by integrating the mass function, Equation 5, over all redshifts:

$$\frac{dN(>T)}{dT} = \int_z^{z_{\max}} \frac{dN(M(T, z_f))}{dM} \frac{dM(T, z_f)}{dT} \frac{dp(z_f)}{dz_f} dz_f, \quad (6)$$

where z_{\max} is the redshift at which Comptonization will efficiently cool virialised haloes. The value of $z_{\max} = 7$ is adopted, but the results are insensitive to this choice for reasonable values (i.e., $z_{\max} > 5$). The cumulative temperature function $N(>T)$ is obtained by numerically integrating Equation 6 over T . Thus, a relationship between mass and temperature is required, and this will depend on the thermal history of the ICM. An analogous procedure is followed to derive the luminosity function, given a relationship between luminosity and mass.

3 MODELS

A singular, truncated isothermal sphere will be assumed for the dark matter potential, $\rho(r) = \rho_R(r/R_{\text{vir}})^{-2}$, where ρ_R is the density at the virial radius, R_{vir} , and is equal to a third of the mean density *within* R_{vir} , $\bar{\rho}(R_{\text{vir}})$. This latter quantity is related to the critical density at redshift z by $\bar{\rho}(R_{\text{vir}}) = \Delta_c(z)\rho_c(z)$, and $\Delta_c = 78\Omega(z) + 80 + 300\Omega(z)/(1 + 15\Omega(z))$ is a fit, accurate to better than 2 per cent, to the results of the spherical collapse model as presented in Eke et al. (1996). It will be convenient to define a redshift evolution term, $F(z)^2 = (1+z)^2(1+\Omega_o z)\Delta_c(z)/\Delta_c(0)$, so that

$$\rho_R = \frac{1}{3}\Delta_c(0)\rho_c(0)F(z)^2. \quad (7)$$

For $\Omega_o = 1$, $F(z)^2 = (1+z)^3$ and $\Delta_c = 178$.

The mass M of a cluster *at its formation redshift* z_f will be defined as the mass within R_{vir} . Thus, the circular velocity V_c , which is independent of r , is given by $V_c^2 = GM/R_{\text{vir}}$. The virial temperature is related to V_c by

$$\begin{aligned} kT_{\text{vir}} &= \frac{1}{2}\mu m_H V_c^2 \\ &= 3.1 \left(\frac{V_c}{1000 \text{ km s}^{-1}} \right)^2 \text{ keV}. \end{aligned} \quad (8)$$

From $M = 4\pi\rho_R R_{\text{vir}}^3$ the following relations are obtained:

$$\begin{aligned} M &= V_c^3 (4\pi\rho_R)^{-1/2} G^{-3/2} \\ &= 2.46 \times 10^{14} h^{-1} F(z_f)^{-1} \left(\frac{\Delta_c(0)}{178} \right)^{-1/2} \left(\frac{V_c}{1000 \text{ km s}^{-1}} \right)^3 M_\odot \end{aligned} \quad (9)$$

and

$$\begin{aligned} kT_{\text{vir}} &= 0.5G\mu m_H(4\pi\rho_R)^{1/3}M^{2/3} \\ &= 1.69h^{2/3}\left(\frac{\Delta_c(0)}{178}\right)^{1/3}F(z_f)^{2/3}\left(\frac{M}{10^{14}M_\odot}\right)^{2/3}\text{keV}. \end{aligned} \quad (10)$$

The volume emissivity of the X-ray emitting gas at radius r is given by

$$\epsilon(r) = \frac{3}{2} \frac{\rho_g}{\mu m_H} \frac{kT_g(r)}{t_{\text{cool}}}, \quad (11)$$

where $T_g(r)$ is the gas temperature, and t_{cool} is its cooling time. For the latter, a fit (Peacock 1996) to the cooling function of Raymond, Cox & Smith (1976), constructed for an H and He plasma with $Y = 0.25$ ($\mu = 0.59$) and incorporating cooling due to both bremsstrahlung and recombination, is implemented. Recombination radiation is important for haloes with $kT < 4$ keV, and its inclusion allows us to consider the mass regime of galaxy groups. The expression for the cooling time is

$$t_{\text{cool}}(r) = \frac{C_1\mu m_H T_g(r)^{1/2}}{\rho_g(r)[1 + C_2 f_m / T_g(r)]} \quad (12)$$

where $C_1 = 3.88 \times 10^{11} \text{ s K}^{-1/2} \text{ cm}^{-3}$, $C_2 = 5 \times 10^7 \text{ K}$ and f_m is a metallicity dependent constant that is 1.0 for solar metallicity (adopted here), and 0.03 for zero metallicity. We only consider haloes in which not all of the gas within R_{vir} has had time to cool since the halo formed. The luminosity is given by integrating the volume emissivity out to the virial radius:

$$\begin{aligned} L &= \int_0^{R_{\text{vir}}} 4\pi r^2 \epsilon(r) dr \\ &= \frac{6\pi k}{C_1(\mu m_H)^2} \int_0^{R_{\text{vir}}} r^2 \rho_g(r)^2 T_g(r)^{1/2} [1 + C_2 f_m T_g(r)^{-1}] dr. \end{aligned} \quad (13)$$

The final density profile of gas that is accreted by a dark matter halo depends on the density profile of the dark matter itself and also on the difference between the entropy of the virialised and infalling gas components. If the entropy of the infalling gas is low, it will be heated by accretion-shocks to approximately the virial temperature of the halo, T_{vir} ; thus, for our adopted mass profile, the gas distribution will be isothermal. Simulations show that, indeed, cluster temperature profiles are isothermal to within a factor of 2–3 (Navarro, Frenk, White 1996; Eke, Navarro, Frenk 1998). Alternatively, if the gas is pre-heated so that it has a large initial entropy, it will be accreted approximately adiabatically, and the gas profile will be isentropic. The purpose of this paper is to consider the properties of cluster gas under these two extreme scenarios. For the majority of clusters, the true physical process is probably intermediate between these models, with the gas becoming more isothermal and less isentropic with increasing halo mass.

3.1 Isothermal Model

In this model, we make the common assumption (e.g., Eke et al. 1996) that the gas is distributed isothermally, with a temperature equal to the virial temperature of the halo. We include a distribution of formation redshifts and recombination radiation, which are often neglected in studies of this nature. The formation redshift z_f of a halo of *observed* mass M has been defined (§ 2.2) to be the redshift at which the mass was equal to fM . Since the gas temperature is assumed not to change between z_f and the epoch of observation, the observed temperature and mass are related, from Equation 10, by

$$kT_g = 4.58\Omega_c^{2/3}\left(\frac{\Delta_c(0)}{178}\right)^{1/3}\left(\frac{f}{0.75}\right)^{2/3}F(z_f)^{2/3}\left(\frac{M}{M_8}\right)^{2/3}\text{keV}. \quad (14)$$

This gives lower temperatures than the relation of Eke et al. (1996), due to the factor of f ; it is only slightly lower than the normalisation of Pen (1998) which was determined from numerical simulations.

If the gas is dissipationless, its density profile will match that of the dark matter, i.e., $\rho_g(r) = \rho_{g,R}(r/R_{\text{vir}})^{-2}$, and $\rho_{g,R}/\rho_R = \Omega_b/\Omega_o$. To avoid the singularity at $r = 0$ when integrating over the assumed isothermal profile, an arbitrary core radius of $r_c = f_c R_{\text{vir}}$ is adopted with $f_c = 0.1$, such that $\rho_g(r < r_c) = \rho_g(r_c)$.

Evaluating Equation 13 yields the following luminosity–temperature relation:

$$L = 5.83 \times 10^{42} h \left(\frac{\Omega_b/\Omega_o}{0.05}\right)^2 \left(\frac{\Delta_c(0)}{178}\right)^{1/2} F(z_f) \left(\frac{kT_g}{\text{keV}}\right)^2 \left(\frac{4/(3f_c) - 1}{12.33}\right) \left[1 + 4.31 f_m \left(\frac{kT_g}{\text{keV}}\right)^{-1}\right] \text{ergs s}^{-1}. \quad (15)$$

The luminosity can be expressed as the sum of two components L_{brem} and L_{rec} , corresponding to the bremsstrahlung

and recombination radiation, respectively. Substituting T_g from Equation 14, $L_{\text{brem}} \propto M^{4/3} F(z_f)^{7/3}$ and $L_{\text{rec}} \propto M^{2/3} F(z_f)^{5/3}$. For $\Omega_o = 1$, this corresponds to $L_{\text{brem}} \propto M^{4/3} (1 + z_f)^{3.5}$ and $L_{\text{rec}} \propto M^{2/3} (1 + z_f)^{2.5}$.

3.2 Pre-Heated Gas

3.2.1 Principles and Definitions

The equation of state of a polytropic gas is $P = K_o \rho_g^\gamma$, where P is the gas pressure, ρ_g is its density, and γ and K_o are constants. K_o is related to the specific entropy of the gas, S , and the specific heat capacity at constant volume, c_v , by (Sears, Salinger 1975)

$$K_o = \frac{h^2}{2\pi(\mu m_H)^{8/3}} \exp(S/c_v - 5/3). \quad (16)$$

In the isothermal model (§ 3.1), it was assumed that the gas was shock heated to the virial temperature upon accretion onto the dark matter potential; in this case, $\gamma = 1$. At the other extreme, which is the focus of this section, gas with high entropy will be accreted adiabatically, and $\gamma = 5/3$. Evaluation of K_o will be discussed further in § 3.2.2.

The gas density profile is obtained by solving the equation of hydrostatic equilibrium:

$$\frac{dP}{dr} = -\frac{GM(r)}{r^2} \rho_g(r). \quad (17)$$

In principle, M is the mass of both the dark matter and the gas, but we will neglect the contribution of the gas, the mass of which is only a few percent of the total (e.g., White et al. 1993). The resulting gas density profile within the virial radius is

$$\rho_g(r) = \rho_{g,R} [1 + 3A^{-1} \ln(R_{\text{vir}}/r)]^{\frac{1}{\gamma-1}}, \quad (18)$$

$$A = \frac{9}{2} \frac{c_s^2(R_{\text{vir}})}{V_c^2} = \frac{3\gamma K_o \rho_{g,R}^{\gamma-1}}{(\gamma-1)V_c^2}, \quad (19)$$

where $c_s(R_{\text{vir}}) = \sqrt{\gamma K_o \rho_{g,R}^{(\gamma-1)/2}}$ is the adiabatic sound speed at the virial radius. This density gradient is significantly shallower than that of isothermal gas and, as a result, the X-ray surface brightness profile is quite flat near the centre, *producing an X-ray core without requiring a core structure in the underlying dark matter or gas mass distributions*. Assuming $\gamma = 5/3$, we derive the ratio of gas mass to dark matter mass within the virial radius from Equation 18:

$$\frac{M_g}{M} = 0.33 \frac{\rho_{g,R}}{\rho_R} A^{-3/2} e^A \Gamma(2.5, A), \quad (20)$$

where $\Gamma(a, x) = \int_x^\infty e^{-t} t^{a-1} dt$ is the incomplete gamma function.

For an ideal, polytropic gas, the temperature is related to the density by

$$\rho_g = \left(\frac{kT_g}{\mu m_H K_o} \right)^{\frac{1}{\gamma-1}} \quad (21)$$

so

$$T_g(r) = T_{g,R} [1 + 3A^{-1} \ln(R_{\text{vir}}/r)] \quad (22)$$

where

$$kT_{g,R} = \frac{\gamma-1}{3\gamma} \mu m_H V_c^2 A = \frac{2}{3} \frac{\gamma-1}{\gamma} A kT_{\text{vir}} \quad (23)$$

is the gas temperature at the virial radius. Observationally, the mean cluster temperature measured is an emission weighted temperature, given by

$$T_{\text{em}} = \frac{\int \epsilon(r) T_g(r) r^2 dr}{\int \epsilon(r) r^2 dr}. \quad (24)$$

The relationship between T_{em} and $T_{g,R}$ is

$$kT_{\text{em}} = \frac{kT_{g,R}}{A} \frac{\Gamma(5.5, A)}{\Gamma(4.5, A)} \left[1 + \frac{4.31 A f_m}{kT_{g,R}} \frac{\Gamma(4.5, A)}{\Gamma(5.5, A)} \right] \left[1 + \frac{4.31 A f_m}{kT_{g,R}} \frac{\Gamma(3.5, A)}{\Gamma(4.5, A)} \right]^{-1}. \quad (25)$$

The bolometric luminosity is given by substituting the density and temperature profiles from Equations 18 and 22 into Equation 13. The result is (assuming $\gamma = 5/3$):

$$L = \frac{6.3 \times 10^{-4} k^{1/2} V_c^{10}}{[C_1 \mu m_H G \Delta_c(0) \rho_c(0)]^{1.5} K_o^3 F(z)^3} e^A \Gamma(4.5, A) \left[1 + \frac{7.5 k C_2 f_m}{\mu m_H V_c^2} \frac{\Gamma(3.5, A)}{\Gamma(4.5, A)} \right]. \quad (26)$$

3.2.2 Relating K_o to the Gas Temperature

Here we will assume $\gamma = 5/3$. The entropy constant K_o , defined in Equation 16, is then related to the temperature and density of the gas by

$$\begin{aligned} K_o &= \frac{kT_g}{\mu m_H \rho_g^{2/3}} \\ &= 3.70 K_{34} \left(\frac{T_g}{10^6 \text{K}} \right) \left(\frac{\rho_g}{\Omega_b \rho_c(0)} \right)^{-2/3} \end{aligned} \quad (27)$$

where $K_{34} = 10^{34} \text{ ergs g}^{-5/3} \text{ cm}^2$.

The entropy of pre-collapse gas can be increased by heating it to a temperature which will depend on the gas density at the time of heating. We will consider heating the gas at the turnaround time, when the overdense region decouples from the Hubble expansion and begins to collapse; if the heating takes place instead at some later time during the collapse of the halo, the gas density will be higher and the amount of heating necessary will be greater. At the turnaround time, the radius of the halo is equal to twice the virial radius e.g. (Lacey, Cole 1993) and, thus, if we assume the perturbation to be homogeneous, we have

$$\bar{\rho}_{\text{ta}} = \frac{1}{8} \bar{\rho}(R_{\text{vir}}) = \frac{1}{8} \Delta_c(0) \rho_c(0) F(z_f)^2. \quad (28)$$

Therefore, we can relate the entropy to the gas temperature at turnaround, $T_{\text{g,ta}}$, by

$$K_o = 314.8 K_{34} \left(\frac{T_{\text{g,ta}}}{10^6 \text{K}} \right) [\Delta_c(0) F(z_f)^2]^{-2/3}. \quad (29)$$

In the special case of $\Omega_o = 1$, Equation 29 becomes

$$K_o = 0.47 K_{34} \left(\frac{T_{\text{g,ta}}}{10^6 \text{K}} \right) (1 + z_f)^{-2}, \quad \Omega_o = 1. \quad (30)$$

The temperature required to obtain a given entropy decreases for lower values of Ω_o , due to the Ω_o dependence of Δ_c .

3.2.3 The Isentropic Model

Assumptions need to be made about the behaviour of $\rho_{\text{g,R}}$ and K_o to evaluate the parameter A in the equations of § 3.2.1. A simple but physically unmotivated assumption is the one we made in the isothermal model, that $\rho_{\text{g,R}}/\rho_R = \Omega_b/\Omega_o$. We discuss interesting results of two such models in Appendix A, but neither produces an entirely satisfying result. Furthermore, constraining $\rho_{\text{g,R}}$ at $r = \infty$ is not a satisfactory constraint because gas cannot be assumed to be in hydrostatic equilibrium beyond a distance approximately equivalent to c_s/H_o , where H_o is the Hubble constant; this distance is equal to a cluster virial radius within a factor of order unity. Beyond this radius, gas will be infalling and its distribution is not represented by our model.

Instead, we will assume that the entropy constant K_o is independent of halo mass, and that the total mass of gas in the cluster is determined by the amount that could have been accreted at the adiabatic Bondi accretion rate (Bondi 1952), assuming that the accreted gas has already been pre-heated, and accretes isentropically:

$$\begin{aligned} \dot{M} &= 4\pi\lambda G^2 M^2 (\gamma K_o)^{-3/2} \rho_g^{3(5/3-\gamma)}, \\ &\approx 1.86\pi\lambda G^2 M^2 K_o^{-3/2}, \quad \gamma = 5/3 \end{aligned} \quad (31)$$

where $\lambda = 0.25$ is the dimensionless accretion rate and ρ_g and T_g are the density and temperature of the gas being accreted. We assume $\gamma = 5/3$ for the remainder of the derivation. If the simplifying assumption is made that the accretion rate has remained roughly constant, the amount of gas mass accreted by the observed redshift z , $M_g(z)$, can be determined from

$$\frac{M_g(z)}{M} = 0.040 \frac{M}{10^{14} M_\odot} \left(\frac{K_o}{K_{34}} \right)^{-3/2} \frac{t(z)}{10^9 \text{ years}}, \quad (32)$$

where $t(z)$ is the Hubble time at redshift z . Thus, we predict a strong mass dependence of the gas mass fraction, $M_g/M \propto M$, for the lowest mass haloes (see below for the mass limit). There is currently insufficient data available to accurately test this prediction, but there are indications that the gas mass fraction increases significantly from elliptical galaxies to groups to clusters (David, Jones, Forman 1995).

The model gas mass fraction, from Equation 32, will exceed Ω_b/Ω_o for clusters with circular velocities greater

than the critical value V_{crit} :

$$V_{\text{crit}} = 998h^{1/3} \left(\frac{\Delta_c(0)}{178} \right)^{1/6} \left(\frac{\Omega_b/\Omega_o}{0.05} \right)^{1/3} \left(\frac{K_o}{K_{34}} \right)^{1/2} \left(\frac{t(z)}{10^9 \text{ years}} \right)^{-1/3} F(z_f)^{1/3} \text{ km s}^{-1}. \quad (33)$$

For $\Omega = 1$, this corresponds to a halo mass of $M_{\text{crit}} = 3.78 \times 10^{14} h \Omega_b (K_o/K_{34})^{3/2} (1+z_f)^{3/2} M_\odot$. Above this mass limit, the Bondi accretion rate will be ignored, and the condition $M_g/M = \Omega_b/\Omega_o$ will be imposed. This is in reasonable agreement with observations (e.g. Edge & Stewart 1991; Evrard 1998) which show that gas mass fractions are roughly constant among clusters, though there is a considerable amount of scatter. The critical halo mass should be compared with the Jeans mass at the turnaround time, which is defined by

$$M_J = \frac{4\pi}{3} \Omega_o \rho_c(z_{\text{ta}}) \lambda_J(z_{\text{ta}})^3 \quad (34)$$

where the Jeans length is $\lambda_J = t(z)c_s$. Using the relations $t_f = 2t_{\text{ta}}$ and $4(1+z_f)^3 = (1+z_{\text{ta}})^3$, (the latter valid only for $\Omega_o = 1$), the Jeans mass of a halo at turnaround can be expressed in terms of its formation redshift as $M_J = 2.4 \times 10^{14} h \Omega_b (K_o/K_{34})^{3/2} (1+z_f)^{3/2} M_\odot$. Thus, we obtain $M_{\text{crit}}/M_J = 1.6$ which is independent of z_f , K_o and h . Since the Jeans mass, which determines the scale at which pressure effects are important relative to gravitational collapse, is not much smaller than M_b , our assumption of adiabatic Bondi accretion is not unreasonable.

For low mass haloes, with circular velocities less than the critical one given in Equation 33, the constant $\rho_{g,R}$ is defined parametrically (through A) by

$$e^A \Gamma(2.5, A) = 6.85h \left(\frac{\Delta_c(0)}{178} \right)^{1/2} F(z_f) \frac{t(z)}{10^9 \text{ years}}. \quad (35)$$

Thus, the parameter A is independent of V_c , but does depend on the redshift of formation in a non-trivial manner. From Equation 19, this requires $\rho_{g,R} \propto V_c^3$. Since A is independent of V_c then, from Equations 9, 23 and 25 the isothermal M–T relation $T_{\text{em}} \propto M^{2/3}$ is again obtained, but the constant of proportionality changes and the dependence on formation redshift is more complex. Allowing for the fact that, on average, higher mass haloes form at lower redshifts than low mass haloes, the M–T relation will be very slightly modified. The luminosity dependence on mass, however, being more sensitive to the gas distribution, differs significantly from the isothermal case. Considering bremsstrahlung radiation only, for example, $L \propto V_c^{10} F(z)^{-3} \propto T_{\text{em}}^5 F(z)^{-3}$. Thus, the important result is obtained that, by assuming adiabatic collapse of gas and a gas mass fraction which is proportional to the total mass, $L \propto T_{\text{em}}^5$.

For high mass haloes, with circular velocities greater than the critical value, the situation is considerably more complex. To solve $\rho_{g,R}$, the parameter A must be determined from the following equation:

$$e^A \Gamma(2.5, A) = (7.5K_o)^{1.5} \left(\frac{\Omega_b}{\Omega_o} \right) [\Delta_c(0) \rho_c(0)] V_c^{-3} F(z)^2. \quad (36)$$

Thus, A (and, hence, $\rho_{g,R}$) depend on both the mass and formation redshift in a complex manner. Furthermore, Equation 36 is not soluble for all V_c . The left hand side of the equation approaches 1.33 as A approaches zero, which means that solutions can only be found for haloes with circular velocities that satisfy

$$V_c < 1366h^{2/3} \left(\frac{K_o}{K_{34}} \right)^{1/2} \left(\frac{\Omega_b/\Omega_o}{0.05} \right)^{1/3} \left(\frac{\Delta_c(0)}{178} \right)^{1/3} F(z)^{2/3} \text{ km s}^{-1}. \quad (37)$$

The model breaks down because the gas becomes increasingly concentrated toward the cluster centre as mass increases and, eventually, the density at the virial radius becomes zero. Since shock heating is expected to dominate the gas entropy for large masses, this is an acceptable limitation. Alternatively, a solution exists for any mass if the entropy constant K_o is made sufficiently high.

The bolometric luminosity, L , is then determined from Equation 26 after solving for A from Equation 35 or 36. Similarly, the emission weighted temperature is computed from equations 23 and 25. Note that L and T do not scale simply with h , due to the complex h dependence of A .

The restriction on circular velocity presented in Equation 37 can be expressed in terms of temperature and luminosity limits as:

$$kT_{\text{crit}} < 6.9h^{4/3} \frac{K_o}{K_{34}} \left(\frac{\Omega_b/\Omega_o}{0.05} \right)^{2/3} \left(\frac{\Delta_c(0)}{178} \right)^{2/3} F(z)^{4/3} \text{ keV} \quad (38)$$

and

$$L_{\text{crit}} < 1.61 \times 10^{44} h^{11/3} \left(\frac{K_o}{K_{34}} \right)^2 F(z)^{11/3} \left(\frac{\Omega_b/\Omega_o}{0.05} \right)^{10/3} \left(\frac{\Delta_c(0)}{178} \right)^{11/6} \times \left[1 + 0.79h^{-4/3} f_m \left(\frac{K_o}{K_{34}} \right)^{-1} \left(\frac{\Omega_b/\Omega_o}{0.05} \frac{\Delta_c(0)}{178} \right)^{-2/3} F(z)^{-4/3} \right] \text{ ergs s}^{-1}. \quad (39)$$

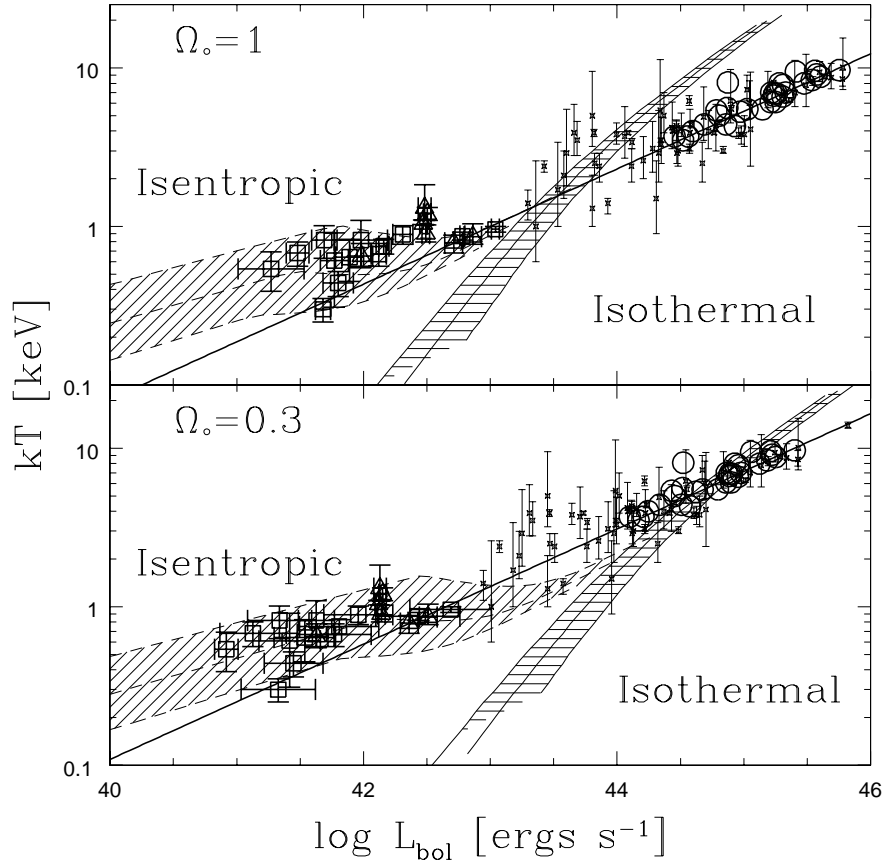


Figure 3. The luminosity–temperature relation, with data from David et al. (1993,1995 stars), Markevitch (1998, circles), Ponman et al. (1996, open squares, resolved sources only) and Mulchaey & Zabludoff (1998, open triangles, Raymond–Smith model determinations with half-solar metallicities). The error bars are omitted from the Markevitch data, as they are smaller than the data symbols. The isothermal model and isentropic model are plotted; the hatched region reflects the range of formation redshifts for clusters of a given mass. Only the isentropic model matches the slope and dispersion of the group data well; the normalisation of this model depends on the initial entropy, which we determine by fitting to the group data. The straight, solid line represents the model of Evrard & Henry (1991). Although this matches the cluster data well, it underpredicts the temperature of low luminosity groups. The models and data do not scale with h in an identical manner, as discussed in the text. The difference between the top panel ($\Omega_o = 1, h = 0.5$) and bottom panel ($\Omega_o = 0.3, h = 0.75$) is due primarily to the different values of h used, and not Ω_o .

4 RESULTS

4.1 The Luminosity–Temperature Relation

The L–T relation[★] for both models and cosmologies is shown in Figure 3; temperature is plotted on the vertical axis, somewhat contrary to convention, since this quantity has the dominant observational uncertainty. For each model, three lines are drawn, representing the range of formation redshifts between $z_f = 0$ and the 1σ upper limit (i.e., where the probability that the cluster formed at a lower redshift is equal to 68.3 per cent). The central line represents the calculation for the most probable formation redshift. The data plotted are those of David et al. (1993;1995, stars), Markevitch (1998, circles), Ponman et al. (1996, open squares)[†] and Mulchaey & Zabludoff (1998, open triangles)[‡]. All data points are unique; where there is overlap we choose the Ponman et al. group data over the Mulchaey & Zabludoff data, and the Markevitch cluster data over that of David et al.

It is crucial to note that the data and models do not scale with h in the same way; for this reason, h has not

[★] The emission weighted temperature of the model is always considered when comparing with observations.

[†] Only fully resolved observations are considered (i.e., with a quality index of 1).

[‡] We use the temperatures determined using the Raymond–Smith model with the metallicity fixed at half solar for all groups except NGC5846, for which this temperature is unconstrained. In this case, we adopt the low metallicity determination.

been left as a free parameter. The observed luminosities scale as $L \propto h^{-2}$, while the isothermal model[§] scales as $L \propto h\Omega_b^2$, from Equation 15. Thus, if Ω_b is fixed, $L \propto h$, while if the big bang nucleosynthesis value is adopted, as we do here, $L \propto h^{-3}$. In either case, the ratio of model to observed luminosity is h dependent. This accounts for most of the difference between the matching of the model and the data in the $\Omega_o = 1$ cosmology (top panel, $h = 0.5$) and the $\Omega_o = 0.3$ cosmology (bottom panel, $h = 0.75$).

The slope of the isothermal model is too steep to match the cluster data, even for haloes with temperatures greater than a few keV. Due to the effects of recombination radiation, it steepens even further for $kT < 4$ keV, approaching $L \propto T$ and, thus, completely fails to match the low-luminosity, group data. Furthermore, for luminosities less than about 10^{43} ergs s⁻¹ the gas will have had time to cool efficiently since the formation of the halo and will no longer be emitting X-ray radiation.

For the isentropic model, the entropy constant, K_o , has been determined by matching the L - T relation to the available group data of Ponman et al. (1996) and Mulchaey & Zabludoff (1998). This constraint requires a value of $K_o = (0.37 \pm 0.1)K_{34}$ which, from Equation 30, can be obtained by heating the gas at the turnaround time to a temperature of about $T = 7.9 \times 10^5(1 + z_f)^2$ K, for $\Omega_o = 1$. For $z_f \approx 1$, the required gas temperature is 3.1×10^6 K; this is reduced to $T = 1.8 \times 10^6$ K for $\Omega_o = 0.3$.

The slope of this model for the lowest masses ($L \propto T^5$) is certainly consistent with most of the group data. Ponman et al. (1996) claim the slope of their data is best fit by $L \propto T^{8.2}$, but there is a great deal of scatter and there are significant outliers. Including the data of Mulchaey & Zabludoff (1998) we obtain a best fit relation of $L \propto T^{3.5}$, but the chi-squared value indicates a poor fit, so the errors on the slope are not well determined. Clearly, more data with smaller errors are required to constrain the slope in this region. It must also be noted that the Ponman et al. (1996) sample is a collection of Hickson compact groups, which are atypical groups. It is, in fact, remarkable that they lie in the same area of the L - T plane as the Mulchaey & Zabludoff (1998) group data.

The change in model slope at $L \approx 10^{42}$ ergs s⁻¹ is due to the change in gas mass constraint, from the amount of mass accreted at the adiabatic Bondi rate to a fixed value (at $V_c = V_{\text{crit}}$; see § 3.2.3). As the halo mass is increased beyond this value, the central gas density increases rapidly, and the gas density at the virial radius drops. Since the density and temperature gradients are initially fairly shallow, the total emission weighted temperature is dominated by the greater volume of gas at large radii; the lower temperature of this gas approximately compensates for the central increase in temperature, and the total emission-weighted temperature remains roughly constant. The luminosity, on the other hand, is more strongly dependent on density and, thus, continues to increase with V_c (although not as strongly as for haloes with $V_c < V_{\text{crit}}$). In this mass regime, the model does not fare as well, generally underpredicting the observed temperatures; this is not unexpected, as accretion shocks will begin to become important for haloes of this size. One possible model for the structure in these haloes is that the pre-heated gas dominates in the central regions, while accretion-heated gas dominates elsewhere. A simple model of this type is described by Evrard & Henry (1991), and is represented by $\log kT = 4/11 \log(h^2 L) - 15.42$ when normalised to the cluster data. This model is shown here as the straight, solid line, which our isentropic model approaches asymptotically. The Evrard & Henry model matches the slope of the cluster data quite well, but underpredicts the temperature of most groups and the lowest mass clusters.

It has been shown (Fabian et al. 1994; Arnaud, Evrard; Markevitch 1998) that the dispersion in the L - T relation can be reduced to a very small value (an r.m.s. dispersion of about 0.11 in $\log L$ at a given T) by excluding cooling flow regions from the observed X-ray data. The predicted (1σ) range in $\log L$ for a given T for high mass clusters under the assumptions of the isothermal model, due to the distribution of halo formation times, is 0.07-0.14, consistent with this data (though, of course, the slope is wrong). The isentropic model predicts a larger range of about 0.3 for low luminosity clusters and groups, and this range encompasses most of the group data shown in Figure 3. This suggests that the observed dispersion in the L - T relation may be primarily due to the distribution of halo formation times.

4.2 The Mass-Temperature Relation

The mass derived from the X-ray temperature of group-scale structures is strongly dependent on the thermal history of the gas, as shown in Figure 4, where the mass-temperature relation is plotted for the isothermal and isentropic models; as in Figure 3, the hatched region represents the dispersion in the relation due to the distribution of halo formation times. At low masses, $M < 10^{13}M_\odot$, the gas mass corresponding to a given temperature is about an order of magnitude smaller in the isentropic model than in the isothermal model: the mass of haloes with $kT < 0.4$ keV will be greatly overestimated by assuming the gas has been accretion-shocked to the virial temperature. Furthermore,

[§] Recall, from § 3.2.3, that the values of L and T in the isentropic model do not scale with h in a simple manner.

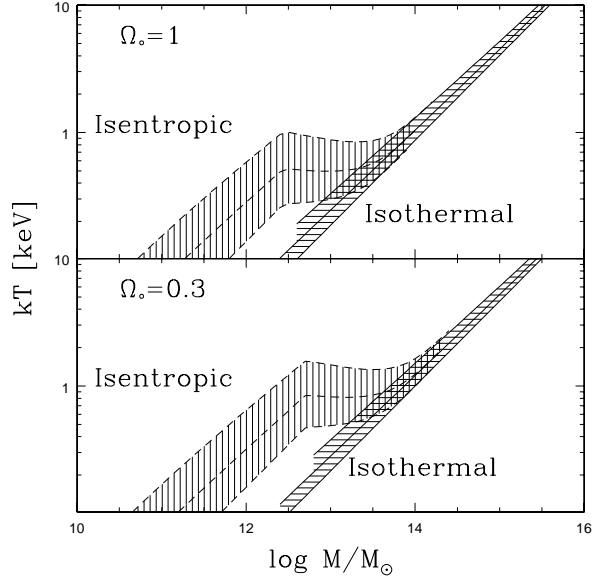


Figure 4. The mass–temperature relations for $\Omega_o = 1$ (top) and $\Omega_o = 0.3$ (bottom). The two models shown in each panel are the isothermal and isentropic models discussed in the text. The hatched region reflects the range of formation redshifts for clusters of a given mass. On the scale of groups of galaxies, both models predict $M \propto T^{1.5}$, but the mass corresponding to a given temperature is an order of magnitude smaller in the isentropic model, compared with the isothermal model.

the dispersion of the M–T relation is significantly larger in the isentropic model; thus it will be difficult to determine the mass of individual, low temperature structures to better than a factor of ten or so from the X-ray observations alone. In the isothermal case, for high temperature clusters, the relation is much tighter, and the mass corresponding to a given temperature can be determined to within a factor of two.

The most readily observable, independent parameter related to the halo mass is the line of sight velocity dispersion, σ_r . Assuming isotropic orbits, we use the relation $V_c = \sqrt{2}\sigma_r$ to compare our model predictions with observations. We show, in Figure 5, the relation between σ_r and gas temperature predicted by the isothermal and isentropic models for $\Omega_o = 0.3$. The group data plotted are the same as in Figure 3; velocity dispersions for the Mulchaey & Zabludoff (1998) are taken from Zabludoff & Mulchaey (1998). For the cluster data, velocity dispersions (not available for all of the data) are taken from Fadda et al. (1996) and various sources within the compilation of White et al. (1997). In the rare cases where uncertainties are not quoted, we assume 20% errors.

The lowest temperature group data generally lie well below the isothermal model prediction; however, there is a great deal of scatter, and insufficient data below $kT = 0.4$ keV to provide a convincing test of our isentropic model prediction. Furthermore, even the massive cluster data tend to lie toward higher temperatures at a given σ_r , which may indicate that the galaxy orbits are not exactly isotropic. The most discrepant point is the cluster AWM4, which seems to have an unusually low velocity dispersion of 119 km/s (Fadda et al. 1996) for its temperature of 3.7 keV. Nonetheless, the data suggest a strong drop in σ_r , relative to the isothermal model, for haloes with temperatures below about 0.8 keV, in accord with our isentropic model. The notable exception to this trend is HCG 15, which has $kT=0.44$ keV and $\sigma_r=457$ km s $^{-1}$ (Ponman et al. (1996)).

The difference between the isothermal and isentropic models in Figures 4 and 5 is somewhat sensitive to the mass accretion rate λ we have assumed in Equation 31. A lower accretion rate (i.e. $\lambda < 0.25$) will preserve the slope of the M–T relation, while altering the normalisation, as the total gas mass within a halo of a given mass will be lower than we have assumed here. In this case, the temperature will drop. Our choice of $\lambda = 0.25$ is the critical value determined by Bondi (1951) for the case of spherical, adiabatic accretion by a point source; we are currently exploring a more realistic accretion model, and indications are that the proper λ may be somewhat lower than we have used here.

4.3 The Temperature Function

The cumulative temperature functions for the two models are shown in Figure 6. The $\Omega_o = 1$ cosmology is shown in the top panel, and the $\Omega_o = 0.3$ results in the bottom panel. The $z = 0$ model is shown as the solid line, and

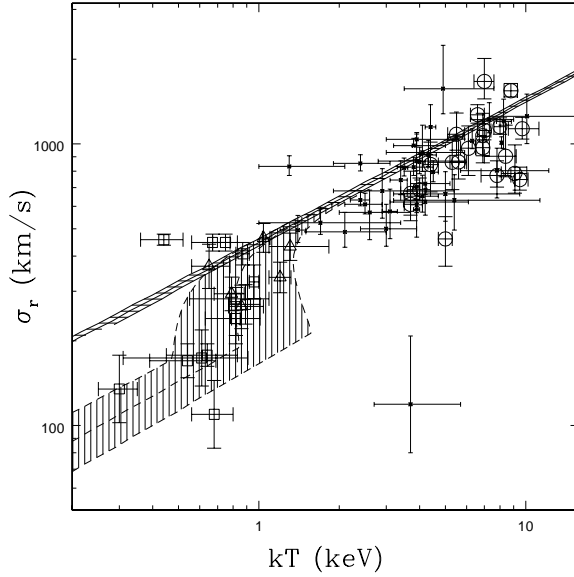


Figure 5. We show the relation between line-of-sight velocity dispersion and gas temperature for the isentropic and isothermal models, with $\Omega_o = 0.3$. The width of the hatched region reflects the range of formation redshifts; the model with the wider band is the isentropic model. The data sources for the temperatures are the same as for Figure 3; sources of the velocity dispersions are described in the text.

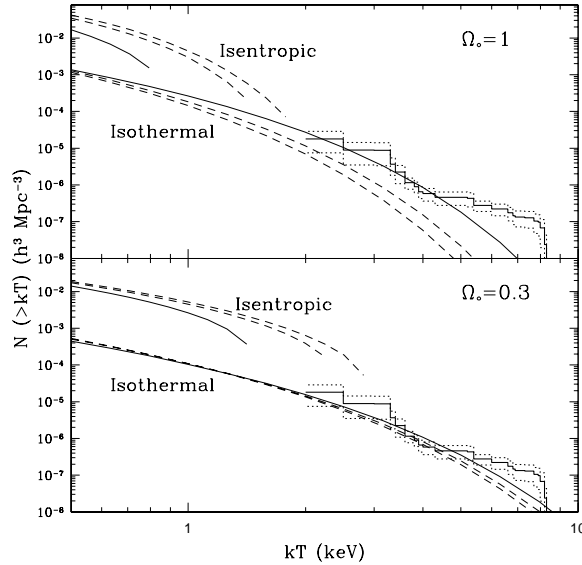


Figure 6. The cumulative temperature function for $\Omega_o = 1$ (top) and $\Omega_o = 0.3$ (bottom). The isothermal and isentropic models are shown at three redshifts, $z=0$ (solid line), $z=0.3$ $z=0.5$ (dashed lines). The $z=0$ models are normalised to the data (Henry & Arnaud 1991, with errors from Pen 1998) at $kT=3.4$ keV. For the isothermal case, evolution at the high temperature end is strongly negative for $\Omega_o = 1$ and only weakly so for $\Omega_o = 0.3$. The isentropic model predicts some positive evolution for objects with $kT < 2$ keV but, as noted in the text (§ 3.2.3), it breaks down for larger mass haloes.

the dashed lines represent the results at redshifts of 0.3 and 0.5. The cluster data from Henry & Arnaud (1991), as analysed by Eke et al. (1996) and with 1σ errors taken from Pen (1998), is plotted as the step function in this figure. This data consists of the 25 X-ray brightest clusters in the *HEAO-1 A2* survey, as detected in the 2–10 keV band.

The *r.m.s.* mass fluctuation in spheres of size $8h^{-1}$ Mpc, σ_8 , is determined by requiring the cumulative temperature function at $z=0$ to match the observations at $kT = 3.4$ keV, where the errors are smallest. For the isothermal model, $\sigma_8 = 0.802$ for $\Omega_o = 0.3$, and $\sigma_8 = 0.492$ for $\Omega_o = 1$. These values are lower than those found by Eke et al.

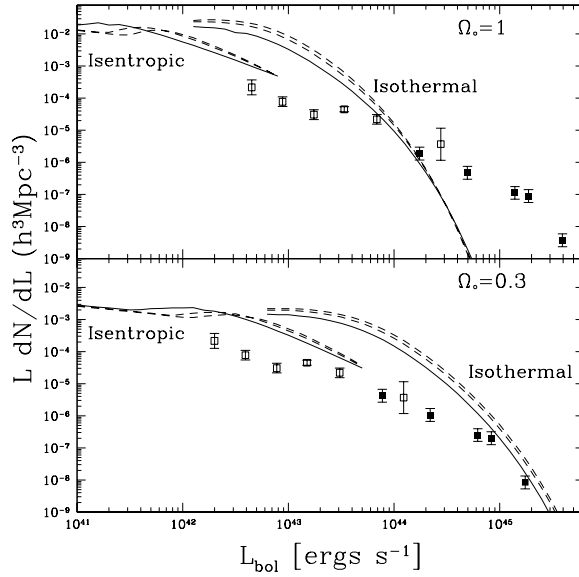


Figure 7. The differential luminosity functions for $\Omega_o = 1$ (top) and $\Omega_o = 0.3$ (bottom). The two models shown in each panel are the isothermal and isentropic models discussed in the text, at $z=0$ (solid line), $z=0.3$ and $z=0.5$ (dashed lines). Very little evolution is exhibited in either model or cosmology. The flattening of the isothermal luminosity function at low L results from efficient cooling of the gas in low mass haloes. The data are from Rosati et al. (1998, open squares) and Henry & Arnaud (1991, filled squares). The normalisation of the models relative to the data is sensitive primarily to the value of h , since the two do not scale the same way.

(1996), primarily as a result of including the distribution of formation times. Neglecting this (i.e., assuming each cluster formed at the redshift at which it is observed) overestimates σ_8 by 10–20 per cent, depending on cosmology (a larger effect for $\Omega_o = 0.3$). The effects of using a slightly different point of normalisation and mass–temperature relation are much weaker, affecting the results by about 1 per cent.

The isentropic model is shown in Figure 6 for the same three redshifts. For this model, σ_8 cannot be calculated in the same way, as the model breaks down for temperatures greater than 1–2 keV, so the values determined above for the isothermal model are used. In this case, evolution is mildly *positive*; i.e., there are more objects of a given temperature at $z=0.5$ than at $z=0$, by a small amount that is roughly independent of cosmology. Relative to the isothermal temperature function, the isentropic model predicts about ten times more objects with temperatures less than 1 keV. This is also evident from Figure 4: the masses of haloes with a given X-ray temperature are much smaller in the isentropic model, and less massive objects are more numerous.

4.4 The Luminosity Function

Although temperature data do not yet exist for a complete sample in the low mass regime, a differential luminosity function is available from the *ROSAT* Deep Cluster Survey (RDCS, Rosati et al. 1998) to luminosities as low as 2×10^{42} ergs s^{-1} . We correct these 0.5–2 keV band luminosities to bolometric luminosities by dividing them by the factor $\exp(-0.5/kT) - \exp(-2/kT)$, where the temperature is estimated from the Evrard & Henry (1991) relation shown in Figure 3. The lowest redshift data from the RDCS ($0.045 < z < 0.25$) are shown as the open squares in Figure 7; the solid squares plotted on this figure are from Henry & Arnaud (1991). The isothermal and isentropic models are shown for both cosmologies. For each model, the solid line is the $z = 0$ model, while the dashed lines represent the results at $z = 0.3$ and $z = 0.5$; very little evolution is exhibited in either cosmology by either model. This is consistent with the RDCS survey results, which show no evolution of the luminosity function out to $z=0.8$.

The slope of the luminosity function corresponding to the isothermal model is too steep to match the data in the high luminosity regime, especially for the $\Omega_o = 1, h = 0.5$ cosmology. As discussed earlier, the normalisation difference between the models and the data is mostly sensitive to h . The flattening of this slope at low luminosities is due to the fact that we do not include haloes in which the gas has had sufficient time to cool since the formation of the halo; efficient cooling in low mass objects restricts luminosities to those greater than about 10^{43} ergs s^{-1} .

The isentropic model, on the other hand, reproduces the flat slope ($d \log(dN/dL)/d \log(L) = -1.88$) of the RDCS data well, though the normalisation is too high. However, the major success of the L–T relation predicted

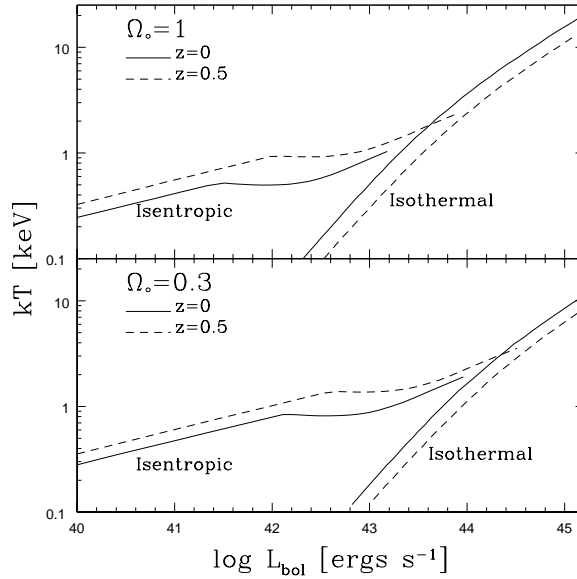


Figure 8. The evolution of the luminosity–temperature relation is shown for $\Omega_o = 1$ (top) and $\Omega_o = 0.3$ for both isothermal and isentropic models discussed in the text. The solid line represents the relation at $z=0$, and the dashed line the relation at $z=0.5$. The (mild) evolution is in opposite directions in the two models.

by this model occurs at luminosities lower than those probed by the RDCS ($L < 10^{42}$ ergs s $^{-1}$) where the gas mass fraction is proportional to the total mass (§ 3.2.3). We predict that the slope of the luminosity function in this mass range will flatten to $d\log(dN/dL)/d\log(L) = -1.33$.

5 DISCUSSION

Recently, Henry (1997) published a detection of mild negative evolution of the cluster temperature function out to $z=0.3$, particularly at the hot end, $kT > 5$ keV. This is marginally inconsistent with the isothermal model in both cosmologies in Figure 6, as the $\Omega_o = 0.3$ temperature function shows too little evolution, while the evolution predicted by the $\Omega_o = 1$ model is too strong. For this reason, Henry (1997) claims $\Omega_o = 0.5$ fits the data best, but there are few points and the error bars are large. The isentropic model predicts very little evolution in both cosmological models, but it is only valid at low temperatures for which there is currently no data. Since the redshift evolution in this case has such a weak cosmological dependence, estimations of cosmological parameters from X-ray abundances will best be made from the number evolution of the most massive clusters, and not from the abundance of lower mass clusters and groups. It is still important, however, to firmly establish the thermal history of the ICM before observed evolution in X-ray luminosity or temperature can be used to determine cosmological parameters.

The direction of evolution of the L–T relation, shown in Figure 8, depends on the gas physics involved. In the isentropic model, clusters of a given temperature are significantly less luminous at $z=0.5$ than they are at $z=0$, whereas, in the isothermal case, they are somewhat more luminous. The work of Henry (1997) shows little or no evolution in the L–T relation for $3 < kT < 10$ keV, in confirmation of earlier work (Henry et al. 1994; Donahue 1996; Mushotzky, Scharf 1997). The prediction of moderate evolution in the isothermal model was part of the impetus for considering models with pre-heated gas (Kaiser 1991; Evrard, Henry 1991); unfortunately, again, our isentropic model is not valid at these temperatures. Since errors in temperature tend to dominate observations, it is unlikely that the predicted evolution of the L–T relation on group scales will be easily observed.

Many observations have suggested that the contribution of X-ray gas to the total mass in galaxy clusters is 10–20 per cent, significantly larger than the Big Bang nucleosynthesis value assumed here (White et al. 1993; White, Fabian 1995; White, Jones, Forman 1997). Increasing the baryon density of the universe allows the application of our isentropic model to more massive haloes, as the limits in Equations 33 and 37 are increased. We explore, in Figure 9, the luminosity–temperature relation assuming $\Omega_b/\Omega_o = 0.1$. (Below our critical mass, Equation 33, the gas mass fraction is still given by Equation 32 and, hence, less than $\Omega_b/\Omega_o = 0.1$, in qualitative accord with observations (David, Jones, Forman 1995)). This requires a slight modification of the entropy constant to $K_o = 0.35K_{34}$ for

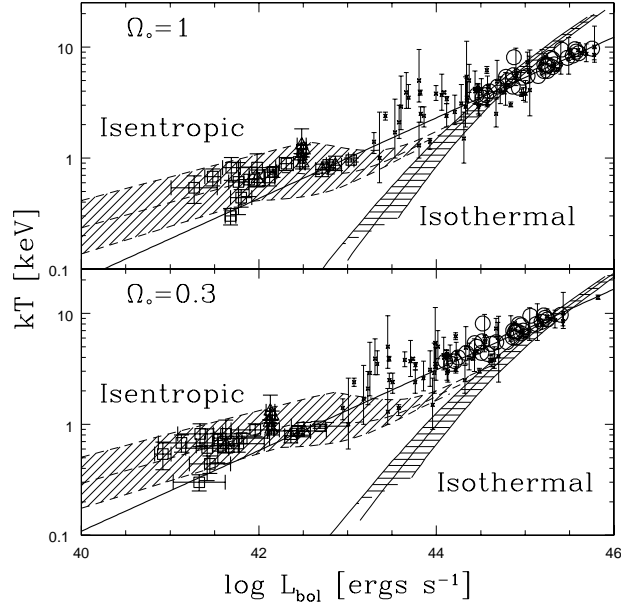


Figure 9. This shows the same models and data as presented in Figure 3, but assuming a larger universal baryon fraction of $\Omega_b/\Omega_o = 0.1$. For $\Omega_o = 1$, the match between the isentropic model and the data is substantially improved.

$\Omega_o = 1$ and $K_o = 0.39K_{34}$ for $\Omega_o = 0.3$. The improvement of the fit to the data is quite noticeable in the $\Omega_o = 1$ case, and is due primarily to the increase of the upper mass limit at which the gas fraction reaches Ω_b/Ω_o .

The isentropic model requires that the infalling gas have an initial entropy given by $K_o = (0.37 \pm 0.1)K_{34}$. This is consistent, with about 1σ confidence, with the observed value recently published by Ponman, Cannon, Navarro (1998), $K_o = (0.20 \pm 0.1)K_{34}$. To generate this entropy requires some mechanism for heating the gas (at the turnaround time) from the background temperature of 10^4 K to about 3×10^6 K (see § 4.1); the energy required to heat a total mass of gas $\Omega_b M$ from $\approx 10^4$ K to this temperature is $1.2 \times 10^{61} (\Omega_b M / 10^{13} M_\odot)$ ergs. If the amount of energy of a single SN event is about 10^{51} ergs, 10 per cent of this is converted into thermal energy of the hot gas (Babul, Rees 1992), and the mass in stars is about 10 percent of the mass in gas, (White et al. 1993), this requires a SN rate of 1.2×10^9 events in the lifetime of a galaxy with stellar mass $10^{10} M_\odot$. Over the likely timescales of galaxy formation, this is probably an unreasonably high rate.

Both models explored here fail to reproduce the temperature function, luminosity function and L–T relation for the majority of massive clusters. This mass range is successfully described in some aspects by the model of Evrard & Henry (1991), in which only the core gas retains its initial entropy, and the possibility of mergers stirring up and mixing the gas is ignored. An alternative model which may be at least equally successful is one in which the gas is more thoroughly mixed, and behaves like a polytrope with γ varying from $5/3$ on group scales to 1.1 – 1.2 on cluster scales, and approaching unity as the systems grow increasingly massive. Such a model has been postulated as an explanation of numerical simulation results (Lewis et al., in preparation), observed temperature gradients (Markevitch et al. 1998) and the discrepancy between X-ray determined masses and those obtained from lensing observations (Miralda-Escude, Babul 1995). We are currently exploring the predictions of such a model under the present formalism.

6 SUMMARY AND CONCLUSIONS

Two extreme models of hot intra-cluster and intra-group gas have been considered in detail. In the first model, the gas is distributed isothermally at the virial temperature of the mass. In the isentropic model, the adiabatic collapse of pre-heated gas onto an isothermal potential is considered, with the gas content of the halo constrained by the physics of adiabatic Bondi accretion. In both models we incorporate the Lacey & Cole (1993; 1994) distribution of halo formation times, and also the contribution of recombination radiation to the gas temperature and luminosity. The important conclusions are the following:

- Neglecting the distribution of halo formation times leads to a 10–20 per cent overestimate of the normalisation parameter σ_8
- Neglecting the contribution from recombination radiation has a significant effect on the slope of the luminosity–temperature relation, for $kT < 4$ keV.
- In the isentropic model, we assume the entropy of the pre-infall gas has been increased by some, unspecified mechanism. For haloes with X-ray gas temperatures $kT < 1$ keV, the luminosity–temperature relation in this model is $L \propto T^5$. Both the slope and dispersion (due to the distribution of formation times) of this model are a good match to the available X-ray observations. The fit is improved, especially for $\Omega_o = 1$, if we assume a baryon fraction of $\Omega_b/\Omega_o = 0.1$.
- The isentropic model predicts that the gas temperature in haloes with $M < 10^{12} M_\odot$ will be significantly higher than the virial temperature; thus, making the assumption that the gas is at T_{vir} will lead to an overestimation of the mass by more than an order of magnitude. This discrepancy can be reduced somewhat if the gas accretion rate is lower than the critical adiabatic Bondi rate we have assumed here; however, we still predict that the gas fraction will increase proportionally to the halo mass in this regime.
- The amount of heating required at $z \approx 1$ in the isentropic model is equivalent to heating halo gas at the turnaround epoch to 3×10^6 K for $\Omega_o = 1$ and 2×10^6 K for $\Omega_o = 0.3$.
- The slope of the observed luminosity function is well matched by the isentropic model for $L < 10^{43}$ ergs s $^{-1}$
- The isentropic model fails for more massive clusters, where the gas entropy becomes increasingly dominated by shocks.

As better X-ray observations become available for less luminous, cooler groups of galaxies, the observed slope of the L–T relation in this regime will provide a strong test of the validity of the isentropic model. For the majority of clusters, the gas is clearly not isentropic or isothermal. These objects may be best described either by largely isothermal gas with a high entropy core (Evrard, Henry 1991), by the shock-heating model of Cavaliere et al. (1997), or by a model which treats the gas as a uniformly mixed polytrope with $\gamma \approx 1.2$.

ACKNOWLEDGEMENTS

We are grateful to NYU, where this work was initiated, for their accommodation and hospitality. We would like to acknowledge many fruitful discussions with Nick Kaiser and Julio Navarro, and we are grateful to Ue–Li Pen for providing his unpublished data. MLB appreciates critical readings by J. Navarro and the referee, T. Ponman, which led to substantial clarifications and improvements. AB wishes to acknowledge partial support from NASA Astrophysics Theory Grant NAG 5-4242. MLB and DRP are supported in part by Natural Sciences and Engineering Research Council of Canada (NSERC) research grants to C. J. Pritchett and A. Babul. MLB is also supported by an NSERC postgraduate scholarship.

APPENDIX A:

In this appendix we will discuss two different models in which pre-heated gas collapses adiabatically. We will make two assumptions about the behaviour of $\rho_{g,R}$ and K_o that are different from those which we make for our isentropic model, discussed in § 3.2.3. In both cases, we assume that $\rho_{g,R}/\rho_R = \Omega_b/\Omega_o$, as in the isothermal model.

First, we can assume that K_o is a universal constant, independent of halo mass. Then, from Equations 19 and 20, the ratio of gas to dark matter mass within R_{vir} will vary strongly with V_c , in the sense that more massive clusters will have smaller gas fractions. The gas mass fraction in this case would vary by two orders of magnitude between haloes with $V_c = 300$ km s $^{-1}$ and those with $V_c = 1000$ km s $^{-1}$. However, both observations and theory suggest that the baryon fraction in clusters may be greater than the universal mean, but do not deviate from this value by more than a factor of a few (White et al. 1993; White, Fabian 1995; David, Jones, Forman 1995; Evrard 1997). Thus, we reject this model as improbable on physical grounds.

Alternatively, we can constrain the ratio of gas mass to dark matter mass to be a constant equal to the universal value, $M_g/M = \Omega_b/\Omega_o$. Then from Equation 20, $A=1.03$ is independent of mass and z_f , which requires the entropy constant to scale as $K_o \propto V_c^2$ (from Equation 19). The entropy of the gas will still be constant for any given cluster, but will be higher for larger haloes; this requires a mechanism for pre-heating the gas that is more efficient for more massive haloes. In this case, since the parameter A is constant, $T_{\text{em}} \propto T_{g,R} \propto V_c^2 \propto T_{\text{vir}}$ from Equations 23 and 25 and, thus, the isothermal mass–temperature relation ($T \propto M^{2/3}$, Equation 14) still holds, apart from the normalisation. Furthermore, from Equation 26, recalling that $K_o \propto V_c^2$, it holds that $L \propto V_c^4$ when bremsstrahlung radiation is the dominant emission mechanism and $L \propto V_c^2$ when recombination radiation dominates; consequently,

$L \propto T^2$ and $L \propto T$ for the two cases, respectively. Interestingly, the above scaling relations are exactly the same as those derived in the isothermal case (§ 3.1). The relationships are *not unique* to the isothermal model.

REFERENCES

- Arnaud K. A., Evrard E. A., 1998, astro-ph/9806353
 Babul A., Rees M. J., 1992, MNRAS, 255, 346
 Bardeen J. M., Bond J. R., Kaiser N., Szalay A. S., 1986, ApJ, 304, 15
 Bertschinger E., Jain B., 1993, ApJ, 431, 495
 Bond J. R., Cole S., Efstathiou G., Kaiser N., 1991, ApJ, 379, 440
 Bondi H., 1952, MNRAS, 112, 195
 Bower R. G., 1997, MNRAS, 288, 355
 Cavaliere A., Menci N., Tozzi P., 1998, astro-ph/9810498
 Cavaliere A., Menci N., Tozzi P., 1997, ApJ, 484, L21
 Copi C. J., Schramm D. N., Turner M. S., 1995, Science, 267, 192
 David L. P., Jones C., Forman W., 1995 ApJ, 445, 578
 David L. P., Slyz A., Jones C., Forman W., Vrtillek S. D., Arnaud K. A., 1993, ApJ, 412, 479
 Donahue M., 1996, ApJ, 468, 79
 Edge A. C., Stewart G. C., 1991, MNRAS, 252, 414
 Efstathiou G., Bond J. R., White S. D. M., 1992, MNRAS, 258, 1P.
 Eke V. R., Cole S., Frenk C. S., 1996, MNRAS, 282, 263
 Eke V. R., Navarro J. F., Frenk C. S., 1998, ApJ, 503, 569
 Evrard A. E., 1997, MNRAS, 292, 289
 Evrard A. E., Henry J. P., 1991, ApJ, 383, 95
 Fabian A. C., Crawford C. S., Edge A. C., Mushotzky R. F., 1994, MNRAS, 267, 779
 Fadda, D. Girardi, M., Giuricin, G., Mardirossian, F., Mezzetti, M. 1996, ApJ 473, 670
 Governato, F., Babul, A., Quinn, T., Tozzi, P., Baugh, C. S., Katz, N., Lake, G. 1998, astro-ph/9810189, submitted to MNRAS
 Henry J. P., 1997, ApJ, 489, L1
 Henry J. P., Arnaud K. A., 1991, ApJ, 372, 410
 Henry J. P., Jiao L., Gioia I. M., 1994, ApJ, 432, 49
 Kaiser N., 1991, ApJ, 383, 104
 Kitayama T., Suto Y., 1996a, MNRAS, 280, 638
 Kitayama T., Suto Y., 1996b ApJ 469, 480
 Lacey C., Cole S., 1993, MNRAS, 262, 627
 Lacey C., Cole S., 1994, MNRAS, 271, 676
 Markevitch M., 1998, ApJ, 504, 27
 Markevitch M., Forman W. R., Sarazin, C. L., Vikhlinin A., 1998, ApJ 503, 72
 Miralda-Escude J., Babul A., 1997, ApJ, 449, 18
 Mulchaey J. S., Zabludoff A. I., 1998, ApJ, 496, 73
 Mushotzky R. F., Scharf C. A., 1997, ApJ, 482, L13
 Navarro J. F., Frenk C. S., White S. D. M., 1995, MNRAS, 275, 720
 Navarro J. F., Frenk C. S., White S. D. M., 1996, ApJ, 462, 563
 Peacock J. A., 1996, Lectures delivered at the EADN School The Structure of the Universe Leiden, July 1995, astro-ph/9601135
 Pen U., 1998, ApJ, 498, 60
 Ponman T. J., Bourner P. D. J., Ebeling H., Bohringer H., 1996, MNRAS, 283, 690
 Ponman, T. J., Cannon, D. B. Navarro, J. F. 1998, astro-ph/9810359
 Press W. H., Schechter P., 1974, ApJ, 187, 425
 Raymond J. C., Cox D. P., Smith B. W., 1976, ApJ, 204, 290
 Rosat, P., Della Ceca R., Norman C., Giacconi R., 1998, ApJ, 492, 21
 Sears F. W., Salinger G. L., 1975, Thermodynamics, Kinetic Theory, and Statistical Thermodynamics, 3rd. ed., Mass: Addison-Wesley Pub. Co.
 Somerville R. S., Lemson G., Kolatt T. S., Dekel A., 1998, astro-ph/9807277
 Viana P. T. P., Liddle A. R., 1996, MNRAS, 281, 323
 White S. D. M., Efstathiou G., Frenk C. S., 1993, MNRAS, 262, 1023
 White D. A., Fabian A. C., 1995, MNRAS, 273, 72
 White D. A., Jones C., Forman W., 1997, MNRAS, 292, 419
 White S. D. M., Navarro J. F., Evrard A. E., Frenk C. S., 1993, Nature, 366, 429
 Zabludoff, A. I., Mulchaey, J. S. 1998, ApJ, 496, 39